Impacts of land cover changes and global warming on climate in Colombia during ENSO events

Astrid Manciu[1,2] · Anja Rammig[1] · Andreas Krause[1] · Benjamin Raphael Quesada[2]

Abstract

Colombia is highly vulnerable to climate change which may be intensified due to the climatic effects of regional deforestation. Here, we quantify the impact of historical (1900–2011) land cover changes (LCC) and of global warming during ENSO events (CC) on precipitation, temperature and surface energy balance components by running the Weather Research and Forecasting model WRF v3.9 at 10 km resolution. We find that historical anthropogenic CC causes a mean temperature increase of 0.77 ± 0.02 °C in Colombia, which is more pronounced in high altitudes. Precipitation is enhanced by 0.98 ± 0.30 mm/day ($+9\%$), particularly over forested areas and reduced at the Pacific coast. LCC imply a reduction of precipitation particularly above the Andes (-0.48 ± 0.10 mm/day) and Caribbean Coast (-0.67 ± 0.12 mm/day), where LCC effects dampen CC effects by 24% and 72%, respectively. La Niña tends to intensify LCC and CC effects in the Andes but dampens them at the Coast, roughly by a factor of two compared to El Niño impacts in both regions. At the subregional level, LCC and CC can have impacts of similar magnitude on precipitation highlighting the need to precisely account for both drivers in hydroclimatic assessments. Contrary to almost all observations and similar simulations with climate models, WRF simulates a cooling bias after historical deforestation in Colombia, even with alternative WRF land surface models. We identify two main sources of biases in the default WRF parametrization to explain this inaccuracy: (1) surface shortwave radiation reflected after deforestation is overestimated; (2) associated evapotranspiration loss is underestimated. Improved model representation and validation of tropical vegetation properties are necessary to provide more robust and confident projections.

Keywords Land cover change · Climate change · Surface energy balance · Deforestation · Regional climate modelling

1 Introduction

Since preindustrial times, mean surface air temperature has risen globally by 1 °C due to anthropogenic emissions of greenhouse gases from fossil fuel burning and land use and land cover changes (LCC, IPCC 2018). Especially the tropics are recently experiencing accelerating deforestation rates (Hansen et al. 2013, Song et al. 2018). Deforestation influences climate by reducing carbon stocks and releasing carbon into the atmosphere (Pan et al. 2011), leading to global warming (biogeochemical feedback to deforestation) and by alterations of regional energy, momentum and water fluxes (biophysical feedbacks), which can outbalance biogeochemical effects and lead regionally to net cooling or additional warming (Claussen et al. 2001). Jia et al. (2019) suggest that on a global scale, biogeochemical effects dominate the interplay of both feedbacks. However, the net impacts of LCC highly vary in space and time and may have contrasting consequences depending on latitude (Davin and de Noblet-Ducoudré 2010). Modelling and observational studies suggest that boreal regions experience a cooling of surface air temperature, while lower latitudes show warming in response to local deforestation (Alkama and Cescatti 2016; Findell et al. 2017). Colombia, a megadiversity hotspot and one of the top 12 deforesting countries (FAO 2015), is particularly affected by such LCC impacts, which in tropical countries are expected to amplify the warming from CC. Every year, roughly 180,000 ha (IDEAM 2017, 2018, 2019) of

✉ Benjamin Raphael Quesada
  benjamin.quesada@urosario.edu.co

  Astrid Manciu
  astrid.manciu@gmail.com

[1] TUM School of Life Sciences Weihenstephan, Technical University of Munich, Hans–Carl–von–Carlowitz–Platz 2, 85354 Freising, Germany

[2] Faculty of Natural Sciences, "Interactions Climate-Environment (ICE)" Research Group, Earth System Sciences Program, Universidad del Rosario, Bogotá, Colombia

forests in Colombia are lost due to agricultural expansion, cattle ranching, urbanization and timber extraction. At the same time, the intensity of extreme weather events associated with the El Niño-Southern Oscillation (ENSO), e.g. droughts or floods, is increasing (Ávila et al. 2019; Hoyos et al. 2013). Thus, the question arises of how such climate events and LCC are interacting.

Understanding deforestation and global warming impacts on climatic variables in Colombia is crucial because this country concentrates very high levels of ecosystem services, terrain complexity, species richness and water provision. Modelling this region is challenging because global climate models cannot resolve small-scale terrain complexity inherent to the presence of the three Andean cordilleras (Posada-Marín et al. 2018; Espinoza et al. 2020). Regional Climate Models (RCMs) can represent local, small-scale phenomena more accurately than global General Circulation Models (GCMs) or Earth System Models (ESM). One of the most widely used RCMs is the Weather Research and Forecasting model (WRF) which has proven its capability to dynamically downscale global reanalysis data from coarse to high resolution in good agreement with observations (e.g. Posada-Marín et al. 2018; Caldwell et al. 2009; Lee and Berbery 2012). In complex terrain domains, WRF is considered to produce climatic features even better than the original reanalysis data sets due to more accurate representation of orography (e. g.Heikkilä et al. 2010; Sun et al. 2016; Soares et al. 2012; Gao et al. 2012; Jiménez-Esteve et al. 2018).

To date, no impact study for Colombia exists that evaluates the impacts of LCC on climate at high spatial resolution. Thus, we present here the first high-resolution, dynamical downscaling study investigating LCC and CC impacts in Colombia. We perform sensitivity simulations with WRF v3.9, forcing the model with historical land cover and climate input and compare the results against present-day conditions. Our aims are to answer the following questions:

(1) How do historical LCC and CC influence surface air temperature and precipitation in different regions of Colombia, during ENSO events (2009–2011)?
(2) What is the dominant forcing for regional climate changes in Colombia?
(3) How are land cover changes and global warming impacts modulated by ENSO?
(4) How is the surface energy balance affected by different scenarios of land cover change in Colombia?

2 Materials and methods

2.1 Study site

Colombia is located in the northwest of South America and contains five major biogeographic regions with contrasting biophysical and land cover properties: Colombian Amazon, Caribbean, Pacific Coast, Orinoco plains (*Llanos orientales*) and Andes. The three branches (*cordilleras*) of the Andes, which cross the country in the center and west, confers Colombia a unique and complex orography with altitudes ranging between 5800 m and sea level, resulting in a wide variety of climatic and vegetation zones. Local-scale phenomena such as inter-Andean valley circulations but also large-scale oscillations in the Atlantic and Pacific, interactions with the Amazon and Orinoco basin influence Colombia's climatic variability (Poveda et al. 2011; Espinoza et al. 2020). On the inter-annual scale however, the hydrological variability is dominated by ENSO, with El Niño causing less evapotranspiration followed by less recycled precipitation, consequently fewer river discharges, and less cloud cover which facilitates more radiation and eventually higher temperatures (Poveda et al. 2011). La Niña, the opposing ENSO-phase, has a reversed effect. ENSO impacts the western Andean branch first while the eastern branch is affected with a little time lag and less strong (Poveda et al. 2011). Generally speaking, Colombia experiences a drier and prolonged dry season during El Niño, and a wetter and prolonged wet season during La Niña.

2.2 Model settings

In order to simulate climate response to LCC and CC in Colombia, we use WRF version 3.9.1.1 (Skamarock et al. 2008). This non-hydrostatic, fully compressible and terrain-following sigma coordinate model (Powers et al. 2017) has been proven to perform well in high-resolution regional modelling studies and is one of the world's most widely used numerical weather prediction models. The simulations are executed by the Advanced Research WRF (ARW) dynamical core of wrf.exe. It contains basic dynamical equations for advection, Coriolis, pressure gradient terms, buoyancy and diffusion. Options on microphysics, radiation schemes and planetary boundary layers are set in namelist.input. Lookup tables for soil characteristics and land cover and vegetation properties set important physical features like minimum and maximum albedo per land use category, surface roughness, rooting depth, which the model accesses during the model run.

The simulations are carried out on two regional domains encompassing a large external domain (D01) covering large parts of Central America, Northern South America, Amazon basin, the Caribbean Sea and Eastern Pacific Ocean, along with an internal (nested) domain covering continental Colombian territory (D02, see Fig. 1), excluding the Colombian islands of San Andres, Providencia and Santa Catalina off the coast of Nicaragua.

All simulations are performed from January 1st, 2009 to December 31st, 2011, excluding the first month from the analysis due to spin-up time, covering two major ENSO events with extreme socio-economic consequences in Colombia (El Niño 2009–2010 and La Niña 2010–2011, Hoyos et al. (2013), Comisión Económica para América Latina y el Caribe (2012)) as well as some ENSO-neutral periods (i.e. March-July 2009, March-June 2010 and May–July 2011 For this period, we find an average Oceanic Niño Index (ONI) value (based on the 3-month running mean of SST anomalies in the Niño 3.4 region [5°N-5°S, 120°-170°W]) of − 0.34 (as computed by the Climate Prediction Center: https://origin.cpc.ncep.noaa.gov/products/analysis_monitoring/ensostuff/ONI_v5.php), meaning that our simulation period (2009–2011) is slightly biased towards more representative of weak La Niña/Neutral periods. It appears that Summer 2010-Spring 2011 was characterized by an Eastern-Pacific (EP) La Niña event of Medium grade (although a strong minimum trimestrial ONI of − 1.6) while Summer 2009-Spring 2010 was marked by a Central-Pacific (CP) El Niño event of Medium grade (with an amplitude of 1.7 °C) (Ren et al. 2018).

We used two-way nesting to allow interactions between inner and outer domain which is the recommended method
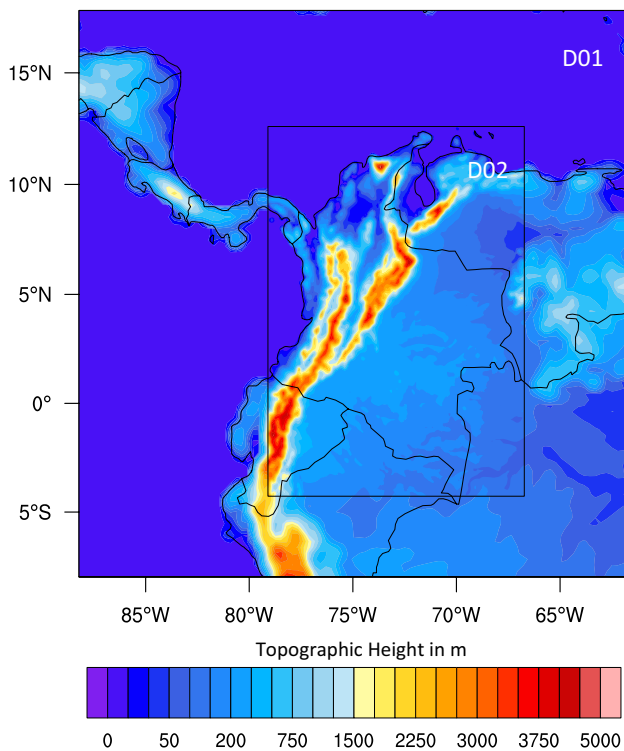

Fig. 1 WPS Domain Configuration and study areas – D01 spans 3000 km×2940 km in zonal and meridional direction and has a resolution of 30 km. D02 spans 1390 km×1900 km and has a resolution of 10 km. Focus regions for analysis are located in the southern Andes and at the Caribbean coast in the north of Colombia

for simulations lasting longer than a few days (Wang et al. 2017). Both domains have 35 vertical levels. D01 has a horizontal resolution of 30 km. A finer 10 km resolution for D02 was chosen as a trade-off between computational time and high resolution of fine-scale climate events. Initial and boundary conditions for the simulations were retrieved from the 6-hourly, 0.75°×0.75° gridded ERA-Interim reanalysis dataset provided by the European Center for Medium-Range Weather Forecasts (ECMWF, Dee et al. 2011).

To avoid large deviations between simulation and driving fields (Bowden et al. 2012) we use spectral nudging on both domains during the whole simulation run, which has been shown to improve simulated results especially in high-resolution downscaling studies (e.g. Chotamonsak et al. 2012; Bowden et al. 2012; Heikkilä et al. 2010). Additionally, Paul et al. (2016) found a reduction in precipitation bias, specifically in rainy regions. Nudging, which comprises relaxation techniques, maintains on the one hand large-scale features from the input data driving field and on the other hand, simulates small-scale features. To let the model develop its own mesoscale and synoptic structures in the surface-near troposphere, we decide to nudge zonal and meridional wind (U and V), temperature (T) and geopotential height (PH) only above the planetary boundary layer additionally to switching off nudging in the first ten levels from the bottom of the model. Similar to Posada-Marín et al. (2018) and Paul et al. (2016), we use a relaxation time of approximately one hour, which corresponds to a value of 0.0003 for U, V, T and PH nudging coefficient (g_{uf}, g_t, g_{ph}). The top wave number, which is the number of waves contained in the domain, is set to three in x and y direction, with three being the maximum one that is nudged, to capture ERA-Interim features with wavelengths of approximately 1200 km and upwards (the WRF domain size is about 3000 km×2940 km in zonal and meridional directions, respectively). Nudging is exerted every 6 h, which coincides with the frequency of our ERA-Interim reanalysis data.

We also rely on previous WRF studies in Colombia or in nearby countries that tested several microphysics, cumulus, longwave radiation, and planetary boundary layer schemes (Arregocés et al. 2021; Núñez 2014; García 2014; Posada-Marín et al. 2018; González-Rojí et al. 2022) to optimize our CTRL configuration. However, the sensitivity of our results to an exhaustive panel of WRF schemes is beyond the scope of this study. In consequence, further physical parametrization schemes considered include the microphysics scheme of the WRF single moment 6-class (Hong and Lim 2006), the new version of the Rapid Radiative Transfer Model (RRTMG) for shortwave and longwave radiation (Iacono et al. 2008), the Noah land surface model (Tewari et al. 2004), the Monin–Obukhov similarity scheme for the surface-layer (Jiménez et al. 2012) and the Yonsei University (YSU) planetary boundary layer (Hong et al. 2006) as
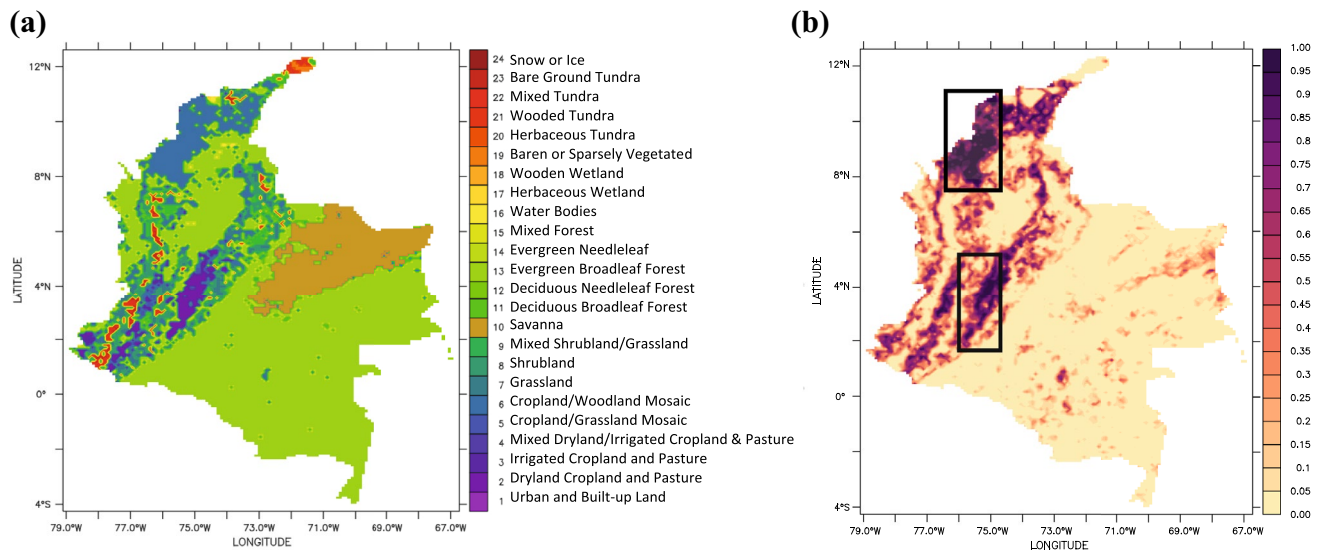
Fig. 2 **a** Land cover in Colombia as used in WRF based on USGS-24-category classification and **b** Extent of land use change in Simulations 2 and 4 (given is the landcover fraction changed in percent) and selection for regional analysis

well as the Kain-Fritsch (KF) scheme cumulus convection parametrization (Kain 2004). We use adaptive time-stepping to avoid the model run crashing when calculating too high windspeed on steep slopes.

We stress here that those model settings (simulation months, schemes, boundary conditions, spin-up, nudging) are similar to the ones used in other recent studies on the detection or attribution of regional and local climatic events, and this standard nudging setting strongly limits the overall model internal variability across simulations (Teklay et al. 2019; Wang et al. 2020; Glotfelty et al. 2021; Lu et al. 2021). Meanwhile, across the simulation period, we find no significant drift in the differences between simulations (<5%, not shown) and we perform sensitivity experiments in Sect. 4.4 to albedo parametrization and physical schemes to explain responses and potential biases.

2.3 Experimental setup

In total, we conduct five main simulations, each one representing a different land cover and/or climate input, for both domains:

(1) CTRL simulation:
    forced by ERA-Interim data for 2009-2011, with standard WRF-built-in land cover map
(2) WITHOUT_LCC simulation:
    forced by ERA-Interim data for 2009-2011, preindustrial land use/land cover (potential natural vegetation)
(3) WITHOUT_CC simulation:

forced by "pseudo anthropogenically-unforced" ERA-Interim data for 2009-2011, with standard WRF-built-in land cover map
(4) WITHOUT_CC_LCC simulation:
    forced by "pseudo anthropogenically-unforced" ERA-Interim data for 2009-2011, preindustrial land use/land cover
(5) 100% DEFORESTATION Simulation:
    forced by ERA-Interim data for 2009-2011 with 100% replacement of forest by cropland and pasture

Those simulations are performed with the same physical parameterization schemes and parameters. Land use categories in the baseline simulation (simulation 1) are based on the USGS land-cover classification (24 categories, see Fig. 2a). For Colombia, this means that it is largely covered by natural vegetation: evergreen broadleaf forest (EBF, Amazonas, Chocó) and savanna (eastern Llanos). Urban and agricultural land is located mostly between the central and the eastern Andean branch, and in the north at the Caribbean coast. According to the built-in USGS land cover classification, only a few pixels are classified as urban and built-up land (Bogotá: 3 grid points; Cartagena, Cali and Barranquilla: 1 grid point, respectively). The most prominent agricultural land use type is dryland cropland and pasture. The Caribbean coast is dominated by a cropland/woodland mosaic.

To retrieve LCC effects on climate, in simulation 2, we changed all categories representing urban and agricultural land to potential natural vegetation (EBF and grassland) classes from inspecting coarse preindustrial land cover maps suggested by Levavasseur et al. (2012) and Hengl et al.

(2018, simulation 2). Each grid cell consists of fractions of more than one land cover type. Therefore, we decide to replace the vegetation properties (minimum and maximum values for albedo, leaf area index, emissivity, roughness length, as well as green vegetation fraction, rooting depth and stomatal resistance) in the classes "Urban and Built-Up land", "Dry cropland and pasture" as well as "Cropland/Woodland mosaic" with the properties of the class "Evergreen Broadleaf Forest". The properties of the classes "Irrigated cropland and pasture", "Mixed dryland/irrigated cropland and pasture" and "Cropland/Grassland Mosaic" are replaced by the vegetation properties of the class "Grassland" (see Fig. 2b).

Simulation 3 is forced by near-preindustrial (~ 1900) ERA-Interim data. 'Pseudo anthropogenically-unforced (PAU)' ERA-Interim data consisted of reconstructing historical climate as if there would be no anthropogenic global warming influence. To achieve this, a three-step approach was employed:

(a) Calculate 30-year monthly mean values for the periods 1900–1929 (~ near-preindustrial) and 1980–2009 (~ present-day) of variables (VAR) needed to force WRF e.g. air temperature, surface pressure, the two wind components and sea surface temperature. 30-year monthly mean values were calculated from the global reanalysis data set ERA-20C, equally provided by the ECMWF.

(b) Calculate the difference between preindustrial and present-day values of VAR.

$$\Delta VAR = VAR_{present-day} - VAR_{pre-industrial}$$

(c) Create for each input variable new ERA-Interim PAU data at each time step:

$$PAU\ ERA\text{-}Interim = ERA\text{-}Interim - \Delta VAR$$

The underlying assumption is that the regional historical trend for those variables is mostly due to anthropogenic global warming forcing. Simulation 4 combines the adjustments made in simulation 2 and 3. The last simulation (simulation 5) represents a complete deforestation (100DEF) scenario which is forced by ERA-Interim data (as in simulation 1 and 2) with dryland cropland and pasture replacing present-day EBF in the whole domain.

2.4 Statistical analysis and visualization

To identify the relative contribution of LCC and CC, the area-weighted mean values of variables over the 3 year-simulation period are calculated at the national level as well as for two focus regions, namely the southern Colombian Andes (76.0°W – 74.8°W, 5.2°N – 1.8°N) between the central and eastern cordilleras, and the Caribbean coast (76.5°W – 74.8°W, 11°N – 7.6°N) in northern Colombia. These two regions were chosen because historically they were particularly affected by LCC (see Fig. 2a, b). Consequently, they presumably exhibit the highest temperature and/or precipitation changes from LCC in the domain.

Simulation 2 to simulation 5 were compared against the CTRL simulation. Hence, the effects were calculated as shown in Table 1.

We calculate the statistical significance of each simulation pair and associated confidence intervals at 95% using a Mann–Whitney-Wilcoxon non-parametric test, commonly used in regional climate studies, without presuming the shape of a variable distribution.

Further analysis focuses on the ENSO phases. Based on the Multivariate ENSO Index (MEI, PSL 2020) and the Oceanic Niño Index (ONI, CPC 2020), the El Niño study period is defined from June 2009 to March 2010, and La Niña from July 2010 to May 2011.

3 Results

3.1 Evaluation of model performance

Since WRF has already been shown to simulate temperatures and precipitation satisfactorily in our model domain (Posada-Marín et al. (2018), we used a similar model configuration and visually evaluated model performance by comparing annual temperature and precipitation to the available observational 30-years average (1981–2010) provided by the Colombian Institute of Hydrology, Meteorology and Environmental Studies (IDEAM 2015). Underlying per-pixel data of the Fig. 3c, d were not publicly available to calculate biases, nor the 2009–2011 average (IDEAM, pers.comm.). However, visually, WRF is representing spatial patterns of annual temperatures satisfactorily (Fig. 3c). Only in the northern lowlands and between the central and eastern Andes

Table 1 Method for calculating the individual effects of land-cover and climate change based on the performed simulation runs

Name of effect	Abbreviation	Calculation performed
Historical LCC effect only	LCC effect	CTRL simulation – without_LCC simulation
Historical CC effect only	CC effect	CTRL simulation – without_CC simulation
Combined effect	–	CTRL simulation – without_CC_LCC simulation
100% Deforestation	100DEF	100DEF simulation – CTRL simulation

valley, it underestimates mean temperature by about 2 °C. WRF simulates peaks higher in altitude (i.e. colder than reanalysis) and valleys lower in altitude on average (i.e. warmer than reanalysis), as expected (see e.g. Figure 11 lower panel of Posada-Marin et al. 2018). Precipitation is generally overestimated across the whole domain but follows the observed spatial patterns.

3.2 Regional impacts of CC and LCC on temperature

In our simulations, global warming (CC) since the beginning of the last century increases regional temperature in Colombia ($+0.77\pm0.02$ °C, Fig. 4b) while historical LCC and 100DEF lead to a significant weak cooling (-0.01 ± 0.01 °C and -0.16 ± 0.01 °C, respectively; Fig. 4a, c). Generally,

(a) Simulated mean annual 2m surface air temperature

(c) Observed mean annual temperature

(b) Simulated mean annual precipitation
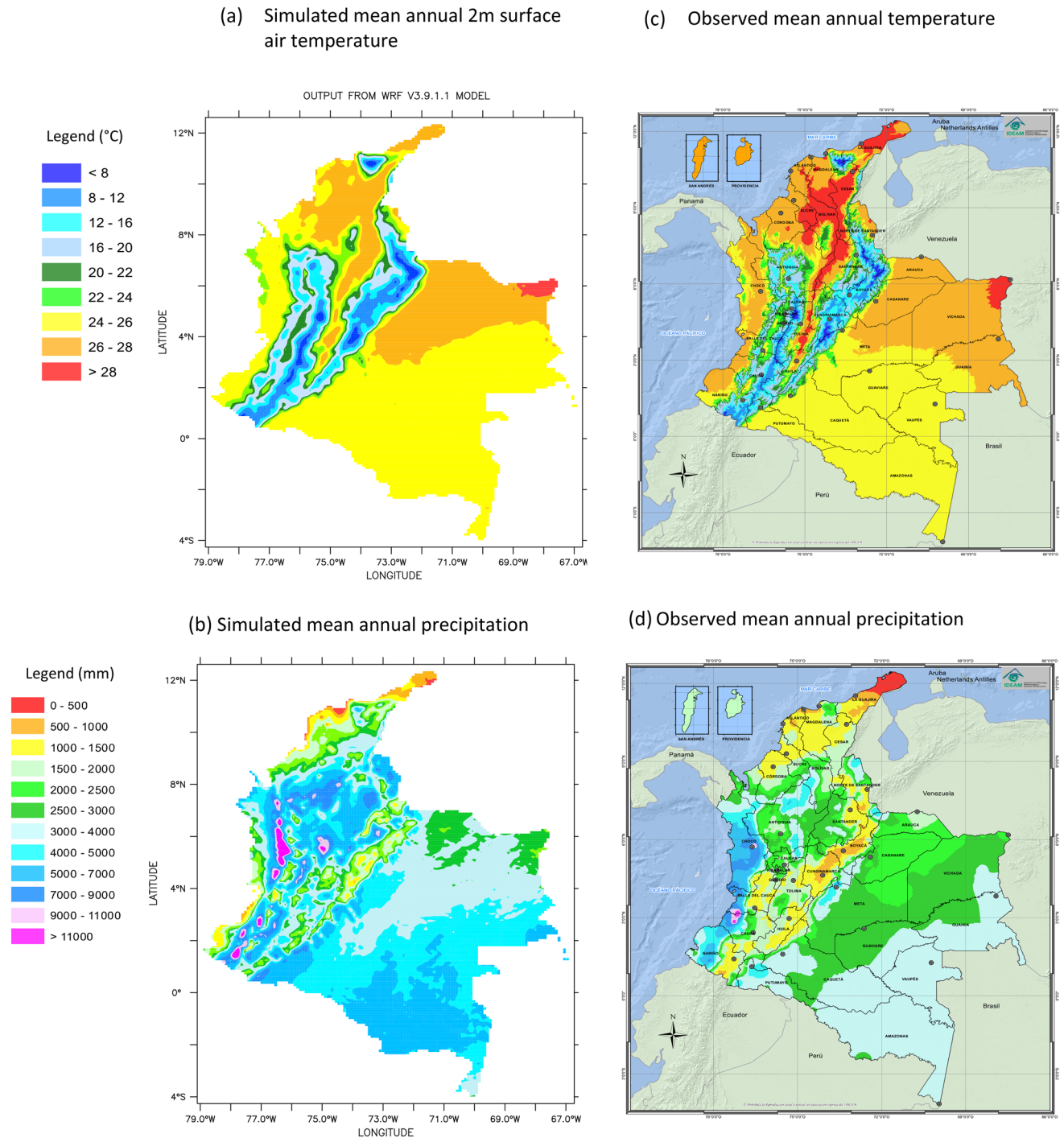
(d) Observed mean annual precipitation

Fig. 3 Model evaluation of **a** simulated mean (2009–2011) annual 2 m surface air temperature and **b** precipitation against **c** observed mean (1981–2010) annual 2 m surface air temperature and **d** precipitation provided by IDEAM. The color scale is the same for both sources

these effects are significantly lower at the Caribbean coast ($+0.58 \pm 0.02$ °C for CC and -0.04 ± 0.01 °C for historical LCC) than in the Andean region ($+0.65 \pm 0.02$ °C for CC and -0.07 ± 0.01 °C for historical LCC). The maps show that the cooling effect from historical LCC is mainly located in the Andean region over potentially historically deforested areas, where forest was converted to cropland and pasture (Fig. 4a). CC effects are significantly stronger at higher altitudes ($+0.17$ °C/km above 500 m at the national level and $+0.12$ °C/km across an Andean transect, $r > 0.6$ for both, in elevation-dependent warming vs. height diagram, see Fig. 5a, b).

Fig. 4 Changes in 2 m surface air temperature (in °C) due to **a** LCC effect, **b** CC effect, **c** 100% deforestation effect and **d** combined effect (LCC+CC). Minimum and maximum values are displayed above and below the color scale

3.3 Regional impacts of CC and LCC on precipitation

Historical LCC and 100DEF simulations both reduce mean precipitation in Colombia by -0.08 ± 0.22 mm/day (− 0.7%, not significant p > 0.05). In contrast, precipitation significantly increases due to CC by 0.98 ± 0.30 mm/day (+ 9%). Combined effects are marginally smaller (+ 0.91 ± 0.31 mm/day) with negligible synergistic effects. In terms of precipitation response, the Caribbean Coast is more affected by historical LCC and 100DEF than the Andean region. In the coastal region, LCC decreases precipitation by − 0.67 ± 0.12 mm/day (− 7%), while 100DEF leads to an increase of 0.44 ± 0.13 mm/day (+ 5%). In contrast, the CC impact is by a factor of two higher in the Andes than at the coast and at the national level. LCC and 100DEF both decrease precipitation in the Andes by − 0.48 ± 0.10 mm/day (− 4%) and − 0.18 ± 0.08 mm/day (− 1.5%), respectively (see Fig. 6a–d). Deforested areas clearly show precipitation reduction (Fig. 6a, c), while CC and combined effects show opposite trends, except for the

Caribbean coast. Precipitation increase is also significantly higher at higher elevations, albeit less significantly than temperature (r < 0.3): by + 0.17 mm/day/km above 500 m at the national level and by + 0.32 mm/day/km across the Andean transect (Fig. 5c, d).

3.4 LCC and CC impacts on temperature and precipitation modulated by ENSO

When comparing simulated temperature changes in Colombia during ENSO events over the study period (mean over 2009–2011), no remarkable differences are found during El Niño (07-2009/03-2010) and La Niña (06-2010/05-2011; see Fig. 7a). The same holds true for the Coast (Fig. 7b). In the Andean region, LCC and CC effects are slightly enhanced in magnitude during La Niña (by − 0.01 ± 0.01 °C –i.e. + 14%– and by + 0.04 ± 0.01 °C –i.e. + 6%– respectively, compared to the full simulation period, Fig. 7c) and dampened during El Niño (− 0.02 ± 0.01 °C – i.e. − 28%– and − 0.08 ± 0.01 °C – i.e. − 12%–, respectively).
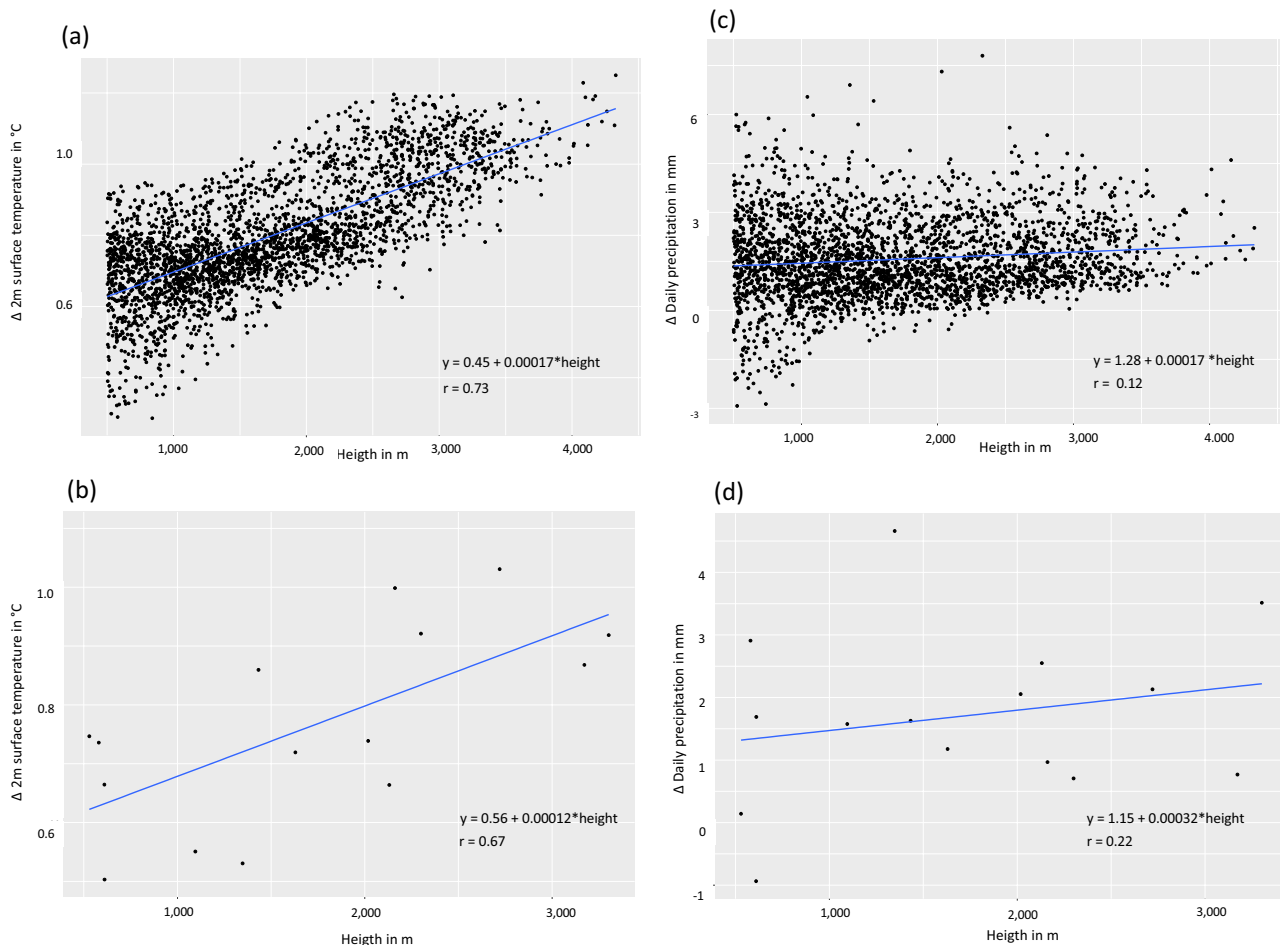

Fig. 5 Relationship between CC-induced temperature/precipitation and altitude. Temperature (**a**, **b**) and precipitation (**c**, **d**) changes across different altitudes above 500 m on national level (upper panels) and across a longitudinal transect (lower panels)
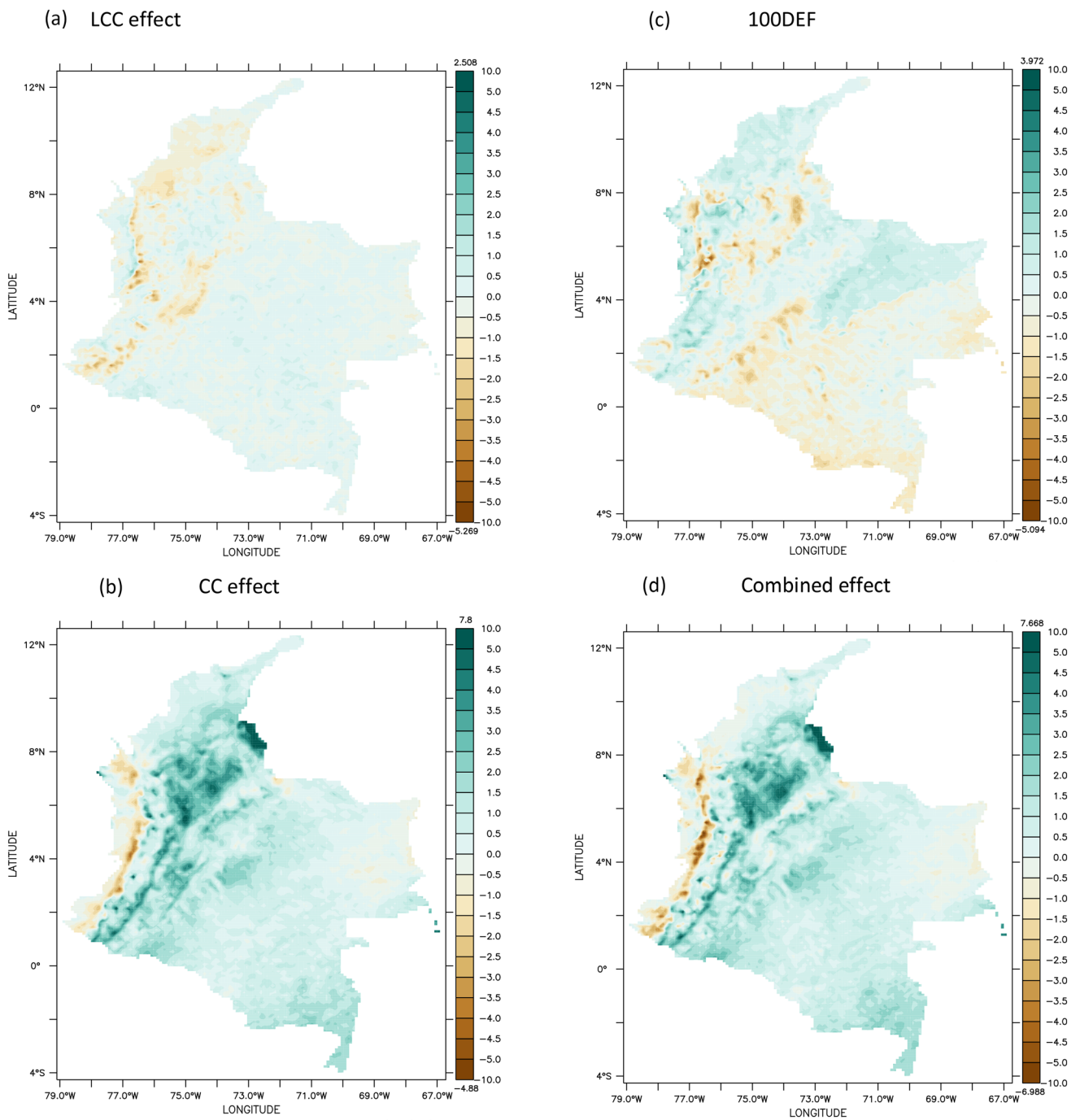
Fig. 6 Same as Fig. 4, but for changes in daily precipitation (in mm)

The CC effect on precipitation depends on the ENSO phases: it is weakened by El Niño ($+0.62 \pm 0.31$ mm/day) but enhanced by La Niña ($+1.08 \pm 0.42$ mm/day, Fig. 7d). Combined effects respond in the same pattern, although slightly weaker than the CC effect ($+0.55 \pm 0.29$ mm/day and $+1.0 \pm 0.4$ mm/day, for El Niño and La Niña respectively). The Andean region reacts in a similar pattern, just about twice as strong in

magnitude (Fig. 7f). At the coast, an opposite reaction can be observed: CC and combined effects are stronger during El Niño and weaker during La Niña (Fig. 7e). Here, historical LCC reduces precipitation, especially during La Niña (-0.84 ± 0.13 mm/day). If the complete domain would be deforested and replaced by dryland cropland and pasture, it would result in a general decrease in precipitation which would hit the Andes the

(a)

(d)

(b)

(e)

(c)

(f)

Fig. 7 Temperature (**a**–**c**) and precipitation (**d**–**f**) changes due to LCC and CC in different Colombian regions: **a** and **d** Colombian mean, **b** and **e** coastal mean, **c** and **f** Andean mean

strongest during La Niña event (-0.23 ± 0.09 mm/day, Fig. 7f). On the contrary, the 100% deforestation case increases precipitation at the coast across all studied time periods, with its highest impact during La Niña ($+0.69 \pm 0.19$ mm/day, Fig. 7e).

3.5 Regional impacts of historical LCC and 100DEF on surface energy balance

Changes in the surface energy balance following historical LCC show a significant increase in $\Delta SW \uparrow$ of 2.03 W/m^2 (p < 0.05, Fig. 8a), resulting in a relative cooling effect.

This represents a contribution of roughly 35% to the total magnitude of change (i.e. $\Delta SW \uparrow$ divided by Δ sum of all absolute flux changes).

A similar change in magnitude but with an opposite sign for ΔL (-1.92 W/m^2, p < 0.05) has a warming effect on national level, thereby balancing the cooling from $\Delta SW \uparrow$. $\Delta(H + G)$ decrease and contribute also to warming, albeit the effect is smaller. Together, the heat fluxes account for 50% of the total magnitude of change (same as above: Δ non-radiative fluxes divided by Δ sum of all absolute flux changes).

Downward radiative fluxes are slightly decreased and contribute around 15% to the overall change. However, on a local scale, changes in fluxes due to LCC effects are imbalanced, especially at the coast, where the dominant land cover was changed from EBF to a cropland/woodland mosaic ($\Delta SW \uparrow$: $+12.43$ W/m^2 vs. ΔL: -9.96 W/m^2; p < 0.05). In the Andean region, where EBF was converted to dryland cropland and pasture, these two fluxes are similarly imbalanced ($\Delta SW \uparrow$: $+6.80$ W/m^2 vs ΔL: -4.26 W/

m^2, p < 0.05), pointing to a dominance of albedo-driven cooling.

The 100DEF scenario with the replacement of all EBF by cropland and pasture in the model domain (Fig. 8b) reveals a more drastic picture compared to historical LCC: a stronger increase in reflected shortwave radiation from the surface and a smaller reduction in latent heat, which is strongest on country level. The effect exists also in the focal regions, though weaker because these areas are already largely deforested in the control simulation.

Albedo on average significantly rises by 0.008 and 0.04 following historical LCC and 100DEF in Colombia, respectively. At the coast, the albedo increases by 0.045 due to historical LCC and by 0.01 under 100DEF. The Andean region shows an albedo increase of 0.02, respectively, after LCC and complete deforestation.

4 Discussion

This study explores the effect of both land cover change and global warming particularly during ENSO events, as well as their combined effects on surface air temperature, precipitation and surface energy fluxes, over Colombia, a climate modeling coldspot.

The performance of the WRF model in simulating general temperature and precipitation patterns in Colombia is satisfactory for the purpose of this research (Fig. 3; Sect. 3.1). An apparent overestimation of precipitation is found comparing our WRF CTRL simulation and IDEAsM patterns (the national observational dataset, see Fig. 3). This can be explained because ERA-Interim already slightly overestimates precipitation in Colombia (Posada-Marín et al. 2018), our large-scale climatic input data to WRF. In addition, Jin et al. (2010) and Teklay et al. (2019) explored different model configurations with varying land surface models (LSM) in a similar context and found that precipitation is overestimated regardless of the LSM used. Another reason for the discrepancy might be the simulation period of only three years of the recent decade.

4.1 CC effect on temperature and precipitation

Interestingly, our results on temperature changes substantially contrast with the official climate near-term projections from the Colombian IDEAM in its Third National Communication on Climate change in Colombia (TCNCC, IDEAM et al. 2017). Historical surface air temperature increases in our study compare well with national averages published by IDEAM ($+0.77$ °C vs. $+0.8$ °C), however, spatial warming patterns are very different (Fig. 4b, d). Our simulations show the highest temperature increases occurring above Andean
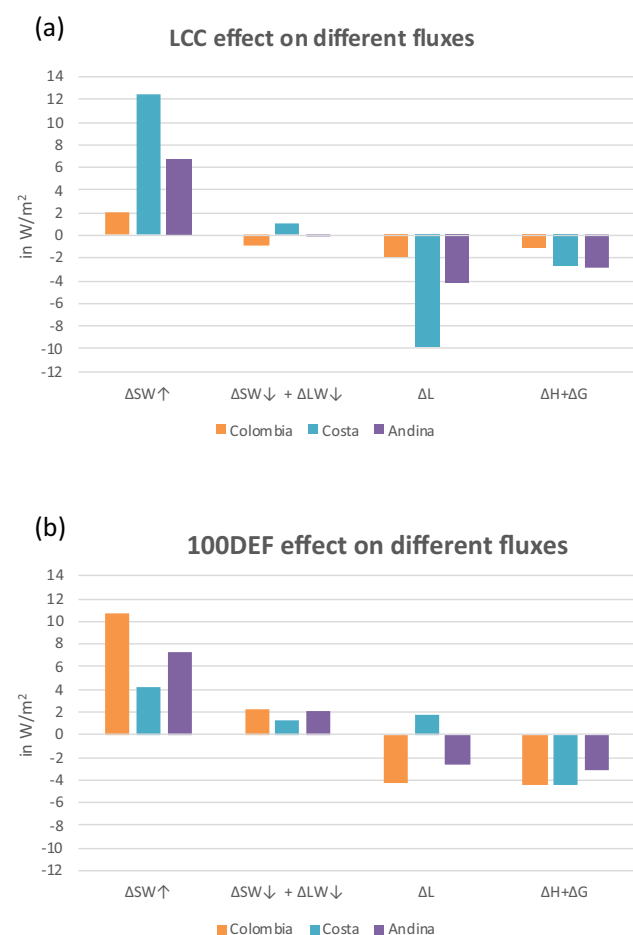

Fig. 8 a LCC and b 100DEF effect on different surface energy fluxes: Shortwave reflected ($\Delta SW \uparrow$), downward fluxes ($\Delta SW \downarrow + \Delta LW \downarrow$), latent heat flux ($\Delta L$), sensible and ground heat flux ($\Delta H + \Delta G$)

cordilleras and higher elevation areas (> 1 °C, dark red in Figs. 4b, d and 5a, b), lower temperature increases in the northern and western areas and intermediate increases in the south and eastern parts (e.g. Llanos and Amazon Forest). This is in contradiction with IDEAM results where higher elevation areas warm less (1–1.5 °C) and the Llanos or low elevation areas more but more homogeneously (> 1.5 °C, Fig. 4b, d). In other means, we show a positive elevation-dependent warming (EDW) while the IDEAM showed the opposite result (negative EDW). Confusingly, the IDEAM states in this very same TCNCC, that the "*most significant increase in mean, minimum and maximum temperatures will be in the Andean region, especially in high elevation areas*" (IDEAM et al. 2017). In the literature, there is growing recent evidence that the rate of warming is amplified with elevation (Pepin et al. 2015; Wang et al. 2016; Hock et al. 2019). However, in the tropics, there is a particular problem with observational data from mountain regions, which is both sparse and inhomogeneous (Pepin et al. 2015), and EDW in the Tropical Andes is controversially discussed in the literature (Vuille and Bradley 2000; Beniston et al. 1997; Hock et al. 2019; Rangwala and Miller; 2012). At least three elements tend to reinforce here our results: (1) most recent literature in the tropics based on observations show more warming above high-elevation vs. low-elevation areas (Rangwala and Miller 2012; Aguilar-Lome et al. 2019), (2) GCMs and RCMs mostly show positive EDW in tropical Andes (Rangwala and Miller 2012; Hock et al. 2019), (3) WRF reproduces correctly the EDW in low latitude environments along elevational gradients (Gao et al. 2018; Expósito et al. 2015; Lin et al. 2015).

Concerning precipitation changes, global warming intensifies the global hydrological cycle (Jia et al. 2019), i.e. the warming of surface air temperature features more evaporation of water into the atmosphere, thus more water content in the air, since warmer air can hold more water vapor. However, according to an average of four emission scenarios, IDEAM et al. (2017) expect precipitation to decrease over the Caribbean coast and the Colombian Amazonas (by 10–40% by 2071–2100 compared to the reference period 1976–2005) and to increase in the Andean region. Our results suggest an overall precipitation increase in Colombia in response to historical global warming, except for the Pacific coast. Our findings are comparable to Skansi et al. (2013), who analyzed station-based time series data from 1950–2010 in South America. Our findings show a drying along the Pacific coast, which is confirmed at least for the southern part by Skansi et al. (2013) but in contradiction to Carmona and Poveda (2014). In WRF, the decrease in Western Pacific Colombian coast precipitation in response to global warming can be explained by less tropospheric winds coming from the Pacific which usually advect moisture, driven by less ocean-continent thermal contrast (not shown).

Furthermore, elevation-dependent rainfall changes under global warming are poorly studied (Li et al. 2017) and we are only aware of one study in the tropics (Urrutia and Vuille 2009, tropical Andes). This latter study does not show consensual patterns of elevation-dependent rainfall changes under global warming, which depends on the latitude or the slope orientation. The authors found that "*In general the projected changes in precipitation are not as pronounced as for temperature*" and that precipitation is slightly higher in the global warming scenario below 4000 m.a.s.l. and slightly less beyond that elevation (Urrutia and Vuille 2009). Our results show a slightly higher rainfall increase under historical global warming in Colombian Andean cordilleras vs. other low-elevation areas (Figs. 5b and 6c, d) which is a consistent pattern with IDEAM near-term projections (IDEAM et al. 2017) and some mid-latitude patterns (Tibetan Plateau, Li et al. 2017) but differs from Urrutia and Vuille (2009).

Finally, our results suggest that CC effects are more dominant on national climate in Colombia than LCC effects while LCC affect rainfall substantially more than temperature at regional and sub-regional scales, which is consistent with most recent studies (Hock et al. 2019; Quesada et al. 2017a, 2017b). Moreover, at the subregional level (Coast or Andean sub-region of Colombia), LCC effects are of the same magnitude on precipitation as CC effects, which urges to systematically account for land-use and land-cover dynamics in any departmental and regional mitigation and adaption to climate change plans.

4.2 LCC effect on precipitation and temperature

A drying over tropical deforested areas is reported throughout the literature (Perugini et al. 2017; Coe et al. 2017; Spracklen and Garcia-Carreras 2015; Lejeune et al. 2015; Saavedra et al. 2020; Sierra et al. 2021; Eiras-Barca et al. 2020) which is in good agreement with our results, although the magnitude of precipitation change differs. Trees usually have a deeper rooting depth and are therefore able to access deep-lying groundwater even in dry periods. Removing tropical forests and replacing them by crops and pastures results in reduced evaporative leaves and canopies, foliar density, surface roughness, stronger winds and an increased albedo. Consequently, evapotranspiration and precipitation (due to fewer clouds) are expected to diminish in tropical agricultural areas. Furthermore, modeled (Sampaio et al. 2007; Nobre et al. 1991; Zemp et al. 2017) changes in precipitation show that drying is even more pronounced during the dry seasons and in low latitude areas.

Reviews on GCM and RCM modeling studies with a focus on Amazon deforestation report a precipitation decrease (Spracklen and Garcia-Carreras 2015; Lejeune et al. 2015; Sampaio et al. 2007). Lejeune et al. (2015) report

a reduction of ~ − 0.7 mm/day (− 5 to − 10%) across 28 GCM and RCM experiments, in agreement with Spracklen and Garcia-Carreras (2015), who report a decrease of 16.5 ± 13% across 44 simulations of complete Amazon deforestation. This is similar to our findings of a 4% decrease in precipitation (− 184 mm/year or − 0.5 mm/day in case of total deforestation over the modeling domain) but more pronounced in magnitude.

Though the comparison with other regional WRF studies (Laux et al. 2017; Paul et al. 2016; Takahashi et al. 2017; Quesada et al. 2017a) shows discrepancies, due to the spatially specific influence of climatic phenomena, they agree that deforestation leads to decreasing precipitation over large-scale deforested areas.

Our simulations show that tropical deforestation causes a slight cooling at country level and more enhanced cooling over deforested grid-cells. Such cooling after deforestation simulated by default WRF parametrizations is at odds against all observations and climate simulations about the tropical deforestation impacts on temperature (Perugini et al. 2017; Lawrence and Vandecar 2015; Jia et al. 2019). The IPCC Special Report on Climate Change and Land (Jia et al. 2019) concludes that there is *high confidence* that large-scale deforestation leads to mean biophysical warming (+ 0.61 ± 0.48 °C) over the entire tropics and especially over deforested areas. After entire Amazon deforestation, GCMs and RCMs reviewed by Lejeune et al. (2015) simulated a temperature increase by 0.8 °C on average, whereas WRF in our study simulates a cooling of − 0.21 ± 0.02 °C over Colombian deforested grid-cells in the 100DEF scenario. Perugini et al. (2017) reviewed eleven modeling studies in the tropics and found a mean temperature increase of 0.68 °C (forest cropland/grassland) which is in agreement with three tropical observational studies they investigated (+ 0.41 °C on average). Temperature changes derived from satellite observations (+ 1.06 °C in Alkama and Cescatti (2016), + 1.34 °C in Duveiller et al. (2018)) or from forest change data (+ 0.38 °C in Prevedello et al. (2019) confirm the warming effect of deforestation in the tropics. However, caution is needed as observational studies do not capture nonlocal biophysical impacts from deforestation (Winckler et al. 2017).

Only a few modeling studies found a cooling as a result of tropical deforestation. For instance, Lejeune et al. (2015) report a mean increase in surface air temperatures of + 1.2 °C across 28 GCM and RCM studies conducted for the Amazon basin with only 3 studies showing cooling out of 28 in total. Robertson (2019), using the HadGEM2-ES ESM, obtained a cooling similar to our study (− 0.08 °C vs. − 0.01 °C) and showed with a decomposition of the surface energy balance that albedo and evapotranspiration responses were strongly biased (overestimated and underestimated, respectively). We suspected similar reasons being responsible for WRF

incorrectly simulating cooling after tropical deforestation and thus conducted in the next section a decomposition of our results as well as sensitivity experiments modifying albedo parametrization and land surface models.

4.3 LCC and CC interactions with ENSO

Studies investigating the interactions between LCC and ENSO in tropical South America are rather rare. The consensus, however, is that LCC enhances the ENSO signal (Nobre et al. 2009; Beltrán-Przekurat et al. 2012; Bush et al. 2017; Zhang et al. 2009). Tölle et al. (2017), for example, used the RCM COSMO-CLM and investigated consequences of abrupt tropical deforestation during the ENSO phases in South East Asia and concluded that they *"can amplify the impact of the natural mode ENSO"*. Another study by Chapman et al. (2020) on the island of Borneo (Indonesia) confirms that deforestation under El Niño conditions resulted in warmer and drier climate than under normal conditions. Syktus et al. (2007), whose study domain was Australia, came to the same conclusion. Bush et al. (2017) suggest that the ENSO signal has been even amplifying since humans started cultivating agricultural goods, which was buffered before by natural vegetation. The buffering effect has been confirmed by Meijide et al. (2018). However, our results suggest that it depends on the region, land cover type, ENSO phase and variable whether the LCC effect is amplified or not, i.e. there is no or little influence of LCC and CC on temperature during ENSO, whereas precipitation changes are more affected, especially during La Niña and at the Coast. Beltrán-Przekurat et al. (2012) concluded from their results that dry periods are enhanced by the occurrence of ENSO, but that the type of land cover conversion also plays an important role for the sign of change.

4.4 Decomposition of energy balance and model sensitivity to albedo parametrization and land surface models (LSM)

At a regional scale, the energy balance is deeply modified by forest losses. In the tropics, a deforestation-driven warming caused by decreased latent heat flux is expected to outbalance the albedo-driven cooling. When decomposing the energy balance into its single components and comparing it to observed values provided by Duveiller et al. (2018), WRF with the coupled Unified Noah LSM (Tewari et al. 2004), which is used here, overestimates the change in reflected shortwave radiation from the surface by a factor of 3.5 over converted grid-cells (EBF → crop/grass, see Table 2). At the same time, the magnitude in latent heat change reduction is underestimated by 41% in WRF. WRF simulates a latent heat flux reduction of 9.6 W/m^2, while a reduction of 20 to 30 W/m^2 would be more realistic according to Duveiller

Table 2 Comparison of simulated deforestation responses in selected variables using different land surface models to observed variables from Duveiller et al. (2018)

Simulation ↓/variable →	$\Delta T2$	$\Delta SW \uparrow$	$\Delta LW \uparrow$	ΔL	$\Delta(H + G)$
Duveiller et al. (2018)	+ 1.34	5.47	7.53	− 16.31	4.21
WRF (Noah, default LSM and albedo)	− 0.07	19.02	1.11	− 9.64	− 8.32
WRF (Noah, default LSM and adjusted albedo)	− 0.03	7.29	2.15	− 2.77	− 5.85
WRF RUC LSM	− 0.13	22.84	− 1.44	− 11.77	− 6
WRF 5 layer thermal diffusion LSM	− 0.13	22.76	− 0.35	− 1.55	− 14.15
WRF Pleim-Xiu LSM	0.06	− 0.02	− 1.4	0.83	0.53

2 m surface air temperature difference is given in °C, energy fluxes in W/m². Values from Duveiller et al. (2018) refer to a mean value for forest—> crop/grass conversions in the tropics, values from model simulations refer to grid-cells with Evergreen Broadleaf Forest—> cropland and pasture conversion

et al. (2018), Nobre et al. (1991) and Snyder et al. (2004) when forests are converted to cropland and/or pasture. Furthermore, sensible heat is decreasing by -8.4 W/m² in WRF following deforestation, instead of increasing by + 5 W/m² to + 20 W/m² as suggested in the literature (Duveiller et al. 2018; Nobre et al. 1991; Sampaio et al. 2007; Llopart et al. 2018; Takahashi et al. 2017; Coe et al. 2017; Oliveira et al. 2019). In summary, the most important reason for the deforestation-temperature bias in WRF seems to be the high overestimation of shortwave radiation reflected from the surface after deforestation, while biases in the latent/sensible heat partitioning tend to compensate each other. This is a coherent finding compared to Sierra et al. (2021) who mentioned the WRF overestimation of the reflected shortwave radiation and the strong underestimation of the sensible heat flux and evaporation/latent heat after cooling in response to forest loss in the tropical Amazon-Andes transition region.

Indeed, Robertson (2019) concluded, that *"to reduce this error the difference between the PFT's albedo parameters should be reduced"*. Following this recommendation, we adjusted the land use category's albedo parameters and ran new WRF simulations. The default albedo ranges from 0.17–0.23 for dryland cropland and pasture, from 0.19–0.23 for grassland and has a constant value of 0.12 for EBF. Observed values for albedo indicate that 0.13 to 0.19 for crops, 0.13 to 0.23 for grassland and 0.11 to 0.15 for tropical EBF are more appropriate (Cescatti et al. 2012, Hänchen 2017; Prentice et al. 1992; Giambelluca et al. 1997). After running simulation 1 and 2 again with these adjusted values (e.g. using minimum albedo of 0.11 and a maximum albedo of 0.15 for EBF), $\Delta SW \uparrow$ is now only slightly overestimated (33%). However, the underestimation of ΔL is amplified (by 83%, see Table 2).

Additional runs were conducted to explore the model's sensitivity to the LSM used. Table 2 shows that the cooling over deforested pixels is even more enhanced when applying the Rapid Update Cycle (RUC) LSM (− 0.13 °C, Benjamin et al. 2004) and the 5-Layer thermal diffusion scheme (− 0.13 °C, Dudhia 1996). Only the Pleim-Xiu LSM (Pleim and Xiu 1995) simulates a warming of

0.06 °C over deforested grid-cells. Furthermore, a decomposition of the alternative LSM's energy balance shows also changes in radiative and non-radiative fluxes that are in stark contrast to observed changes (Duveiller et al. 2018, see Table 2). Thus, we investigated several sources of deforestation-induced temperature biases in WRF, which were found in recent tropical studies performed with WRF in the default configuration (Glotfelty et al. 2021; Sierra et al. 2021).

Finally, we stress here that we are confident with WRF responses to CC (Sect. 4.2) as well as precipitation responses to LCC: (1) vegetation model properties are the same between CC simulations and climatic patterns are well represented by WRF in this region – see Sect. 3.1 and Posada-Marín et al. (2018); (2) precipitation responses after LCC and tropical deforestation (100DEF) are consistent with the observations in this tropical region (see Sect. 4.3), (3) the biases tend to cancel out: the underestimation of evapotranspiration loss after deforestation has an opposite effect with respect to the overestimated cooling for precipitation: the former tends to underestimate the magnitude of the reduced precipitation response (more evapotranspiration leads to more clouds and in turn more precipitation) while the latter tends to overestimate it (cool air tends to hold less water thus less precipitation, Mahmood et al. (2014); (4) across the different WRF land cover schemes tested, precipitation responses are not substantially affected and are systematically negative after deforestation (not shown).

5 Conclusion

Colombian climate regional modelling is challenging in several respects: it has a highly uneven and mountainous terrain highlighting the need for high-resolution modelling, it is a regional climate modelling coldspot (very few studies), it is highly vulnerable territory to climate change and biodiversity loss and thus, it calls for an urgent need of hydroclimatic assessments (Poveda et al. 2011). In this study, we quantified and disentangled the impact of

historical LCC and CC on Colombian climate performing WRF simulations during ENSO events (2009–2011), identifying the most dominant forcing and analyzing the impacts of historical LCC on the surface energy balance given several model configurations.

LCC reduces precipitation everywhere over deforested areas, but especially in the Caribbean coast in the north. Conversely, CC increases precipitation, specifically in the Andean region. LCC effects are found to be strong drivers of sub-regional precipitation changes: dampening CC effects magnitude by 72% and 24% on average in Coastal Caribbean and Andean regions, respectively. Combining historical LCC and CC, temperature increases by 0.76 °C, especially in high altitudes. Conflicting with most other modeling studies and observations, WRF simulates a temperature decrease following historical LCC and 100DEF, which is intensified over deforested areas.

Our results suggest that CC effects are more dominant on regional climate in Colombia than LCC effects but both effects are comparable in magnitude over deforested areas or at the subregional level. La Niña tends to enhance the studied effects across the country, whereas El Niño weakens them, except at the coast where the pattern is mostly inverted. In the Andes, La Niña tends to intensify LCC and CC effects roughly to a factor of two compared to El Niño impacts in both cases.

Our simulations indicate a serious bias in WRF concerning an incorrect simulation of cooling after tropical deforestation, recently found as well in other tropical regions (Glotfelty et al. 2021; Sierra et al. 2021). We further investigate this apparent bias because of its great importance for climate studies using WRF with default parametrization in tropical contexts and probably beyond. We show here that WRF coupled with the Unified Noah LSM, RUC LSM and the 5-layer thermal diffusion LSM overestimates reflected surface shortwave radiation response and underestimates evapotranspiration-driven warming in the tropics which leads us to the assumption that vegetation properties are not appropriately parametrized for tropical regions in all investigated LSMs in WRF. We therefore recommend using default vegetation properties of WRF with caution for temperature assessments. Improved model representation of vegetation properties and more validation data in tropical areas are needed to provide more robust and confident climate projections at regional-to-local scale. We stress here that, although our study has limits concerning the limited sensitivity experiments across physical schemes or imprecise representation of land-cover characteristics, the model settings are tuned to limit internal model variability maximizing the signals response, following similar WRF climatic studies (see Sects. 2.2 and 2.4). Meanwhile, we provide statistical significance to ensure robust messages throughout

this first-of-its-kind attribution study at high-resolution (10 km) analyzing global warming and land-cover changes impacts on climate in this region. Although our simulation period is limited (2009–2011), our results on the whole period are likely to represent the simulated impact of historical land cover changes and global warming on Colombian climate during a climatological period, albeit slightly skewed towards La Niña.

To avoid obvious temperature biases in WRF simulations, in-depth analysis and further development of land cover classification and the representation of vegetation properties used by WRF is necessary. This includes a more realistic and up-to-date representation of tropical land cover data. USGS land use classification in WRF standard simulations dates back to the early 90s. Since then, tropical deforestation and land use rose tremendously. A thorough review of vegetation properties parametrization is necessary to assure a good representation of tropical land–atmosphere feedbacks. We implemented alternative albedo values for Colombia's most important land use categories and tested its sensitivity, which showed a substantial improvement of simulated reflected shortwave radiation. However, parametrizations of e.g. roughness length and stomatal resistance, important parameters which drive evapotranspiration, were not investigated, potentially explaining that simulated latent heat fluxes were even more biased. To understand the role of the ENSO phases better, longer simulation studies are needed, in order to have a more appropriate climatological period and an average of more ENSO events. In addition, a follow-up study could investigate climate extreme indices like maximum daily temperature and maximum daily precipitation to provide evidence for LCC and CC impacts on extreme weather events. Although land use data has been used for regional climate simulations in the Neotropics (e.g. Sierra et al. 2021; Saavedra et al. 2020) and although a more recent update land use data already exists (years 2000s, Eva et al. 2004), a newer high-resolution land-cover dataset for Colombia spanning a climatological period would represent a great input for more robust climate and hydrological assessment in Colombia. Finally, it should be noted that the official climatic projections by the TCNCC (IDEAM et al. 2017) contains methodological shortcomings, inconsistencies and need urgent reassessment by the national communities of meteorology and climatology (Arias et al. 2022).

Declarations

Conflict of interest The authors declare no conficts of interest or competing interests.

References

Aguilar-Lome J, Espinoza-Villar R, Espinoza J-C, Rojas-Acuña J, Willems BL, Leyva-Molina W-M (2019) Elevation-dependent warming of land surface temperatures in the Andes assessed using MODIS LST time series (2000–2017). Int J Appl Earth Obs Geoinf 77:119–128. https://doi.org/10.1016/j.jag.2018.12.013

Alkama R, Cescatti A (2016) Biophysical climate impacts of recent changes in global forest cover. Science 351:600–604. https://doi.org/10.1126/science.aac8083

Arias PA, Villegas LD, Mesa OJ, Pabón JD, Arango J, Santiago, Arango-Aramburo S, Armenteras D, Barahona R, Berrouet L, Barco J, Cardona Y, Carvajal-Escobar Y,Ceballos-Bonilla LI, Cerón WL, Escobar JH, González C, Hoyos IC, Hoyos N, Jaramillo C, Jiménez-Sánchez G, Martínez JA, Poveda G, Quesada B, Quintero-Vallejo E, Rendón Am, Ruiz-Carrascal D, Salazar A, Salazar JF, Sánchez A, Vieira SC, Villegas JC, Villegas-Palacio C, Zuluaga MD (2022) Implicaciones metodológicas e inconsistencias de la Tercera Comunicación Nacional sobre Cambio Climático de Colombia. Revista de la Academia Colombiana de Ciencias Exactas Físicas y Naturales 46(180):769–794. https://doi.org/10.18257/raccefyn.1705

Arregocés HA, Rojano R, Restrepo G (2021) Sensitivity analysis of planetary boundary layer schemes using the WRF model in Northern Colombia during 2016 dry season. Dyn Atmos Oceans 96:101261. https://doi.org/10.1016/j.dynatmoce.2021.101261

Ávila Á, Guerrero F, Escobar Y, Justino F (2019) Recent precipitation trends and floods in the Colombian Andes. Water. https://doi.org/10.3390/w11020379

Beltrán-Przekurat A, Pielke RA Sr, Eastman JL, Coughenour MB (2012) Modelling the effects of land-use/land-cover changes on the near-surface atmosphere in southern South America. Int J Climatol 32:1206–1225. https://doi.org/10.1002/joc.2346

Beniston M, Diaz HF, Bradley RS (1997) Climatic change at high elevation sites: an overview. Clim Change 36:233–251. https://doi.org/10.1023/a:1005380714349

Benjamin SG et al (2004) An hourly assimilation-forecast cycle: the RUC. Mon Weather Rev 132:495–518

Bowden JH, Otte TL, Nolte CG, Otte MJ (2012) Examining interior grid nudging techniques using two-way nesting in the WRF model for regional climate modeling. J Clim 25:2805–2823. https://doi.org/10.1175/jcli-d-11-00167.1

Bush MB, Correa-Metrio A, van Woesik R, Shadik CR, McMichael CNH (2017) Human disturbance amplifies Amazonian El Nino-southern oscillation signal. Glob Chang Biol 23:3181–3192. https://doi.org/10.1111/gcb.13608

Caldwell P, Chin H-NS, Bader DC, Bala G (2009) Evaluation of a WRF dynamical downscaling simulation over California. Clim Chang 95:499–521. https://doi.org/10.1007/s10584-009-9583-5

Carmona AM, Poveda G (2014) Detection of long-term trends in monthly hydro-climatic series of Colombia through empirical mode decomposition. Clim Chang 123:301–313. https://doi.org/10.1007/s10584-013-1046-3

Cescatti A et al (2012) Intercomparison of MODIS albedo retrievals and in situ measurements across the global FLUXNET network. Remote Sens Environ 121:323–334. https://doi.org/10.1016/j.rse.2012.02.019

Chapman S et al (2020) Compounding impact of deforestation on Borneo's climate during El Niño events. Environ Res Lett. https://doi.org/10.1088/1748-9326/ab86f5

Chotamonsak C, Salathe EP, Kreasuwan J, Chantara S (2012) Evaluation of precipitation simulations over Thailand using a WRF regional climate model. Chiang Mai J Sci 39:623–638

Claussen M, Brovkin V, Ganopolski A (2001) Biogeophysical versus biogeochemical feedbacks of large-scale land cover change. Geophys Res Lett 28:1011–1014. https://doi.org/10.1029/2000gl012471

Coe MT, Brando PM, Deegan LA, Macedo MN, Neill C, Silvério DV (2017) The forests of the Amazon and cerrado moderate regional climate and are the key to the future. Trop Conserv Sci. https://doi.org/10.1177/1940082917720671

Comisión Económica para América Latina y el Caribe C (2012) Valoración de daños y pérdidas. Ola invernal en Colombia 2010–2011. Bogotá: Misión BID - Cepal

CPC (2020) Historical El Nino / La Nina episodes (1950-present) [Online]. Boulder, Colorado, USA: NOAA. National Weather Service. Climate Prediction Center. Available: https://origin.cpc.ncep.noaa.gov/products/analysis_monitoring/ensostuff/ONI_v5.php. Accessed 10 Oct 2019

Davin EL, de Noblet-Ducoudré N (2010) Climatic impact of global-scale deforestation: radiative versus nonradiative processes. J Clim 23:97–112. https://doi.org/10.1175/2009jcli3102.1

Dee DP et al (2011) The ERA-interim reanalysis: configuration and performance of the data assimilation system. Q J R Meteorol Soc 137:553–597. https://doi.org/10.1002/qj.828

Dee DP et al (2016) ERA-20C: an atmospheric reanalysis of the twentieth century. J Clim 29:4083–4097. https://doi.org/10.1175/jcli-d-15-0556.1

Dudhia J (1996) A mulit-layer soil temperature model for MM5. The Sixth PSU/NCAR Mesoscale Model Users' Workshop, Boulder, Colorado

Duveiller G, Hooker J, Cescatti A (2018) The mark of vegetation change on earth's surface energy balance. Nat Commun 9:679. https://doi.org/10.1038/s41467-017-02810-8

Eiras-Barca J, Dominguez F, Yang Z, Chug D, Nieto R, Gimeno L, Miguez-Macho G (2020) Changes in South American hydroclimate under projected Amazonian deforestation. Ann N Y Acad Sci. https://doi.org/10.1111/nyas.14364

Espinoza JC, Garreaud R, Poveda G, Arias PA, Molina-Carpio J, Masiokas M, Viale M, Scaff L (2020) Hydroclimate of the Andes part I: main climatic features. Front Earth Sci. https://doi.org/10.3389/feart.2020.00064

Eva HD et al (2004) A land cover map of South America. Global Change Biolology. https://doi.org/10.1111/j.1529-8817.2003.00774.x

Expósito FJ, González A, Pérez JC, Díaz JP, Taima D (2015) High-resolution future projections of temperature and precipitation in the Canary islands. J Clim 28:7846–7856. https://doi.org/10.1175/jcli-d-15-0030.1

FAO (2015) Deforestation in Colombia [Online]. Available: www.globalforestwatch.org. Accessed 19 Feb 2020

Findell KL, Berg A, Gentine P, Krasting JP, Lintner BR, Malyshev S, Santanello JA Jr, Shevliakova E (2017) The impact of anthropogenic land use and land cover change on regional climate extremes. Nat Commun 8:989. https://doi.org/10.1038/s41467-017-01038-w

Gao Y, Fu JS, Drake JB, Liu Y, Lamarque JF (2012) Projected changes of extreme weather events in the eastern United States based on a high resolution climate modeling system. Environ Res Lett. https://doi.org/10.1088/1748-9326/7/4/044025

Gao Y, Chen F, Lettenmaier DP, Xu J, Xiao L, Li X (2018) Does elevation-dependent warming hold true above 5000 m elevation? Lessons from the Tibetan Plateau. npj Clim Atmos Sci. https://doi.org/10.1038/s41612-018-0030-z

García J (2014) Validación de la capacidad del modelo WRF "Weather Research and Forecasting" para pronosticar lluvia intensa, usando el método orientado a objetos y tablas de contingencia. [Master's Thesis, Universidad Nacional de Colombia]

Giambelluca TW, Hölscher D, Bastos TX, Frazão RR, Nullet MA, Ziegler AD (1997) Observations of Albedo and radiation balance over postforest land surfaces in the eastern Amazon basin. J Clim 10:919–928. https://doi.org/10.1175/1520-0442(1997)010%3c0919:Ooaarb%3e2.0.Co;2

Glotfelty T, Ramírez-Mejía D, Bowden J, Ghilardi A, West JJ (2021) Limitations of WRF land surface models for simulating land use and land cover change in Sub-Saharan Africa and development of an improved model (CLM-AF v. 1.0). Geosci Model Dev 14:3215–3249. https://doi.org/10.5194/gmd-14-3215-2021

González-Rojí SJ, Messmer M, Raible CC, Stocker TF (2022) Sensitivity of precipitation in the highlands and lowlands of Peru to physics parameterization options in WRFV3.8.1. Geosci Model Dev 15(7):2859–2879. https://doi.org/10.5194/gmd-15-2859-2022

Hänchen L (2017) Modelling impacts of land-cover changes on temperature Estimation of direct biophysical and biochemical effects using a semi-empirical approach. Master of Science, Leopold-Franzens Universität Innsbruck

Hansen MC et al (2013) High-resolution global maps of 21st-century forest cover change. Science 342:850–853. https://doi.org/10.1126/science.1244693

Heikkilä U, Sandvik A, Sorteberg A (2010) Dynamical downscaling of ERA-40 in complex terrain using the WRF regional climate model. Clim Dyn 37:1551–1564. https://doi.org/10.1007/s00382-010-0928-6

Hengl T, Walsh MG, Sanderman J, Wheeler I, Harrison SP, Prentice IC (2018) Global mapping of potential natural vegetation: an assessment of machine learning algorithms for estimating land potential. PeerJ 6:e5457. https://doi.org/10.7717/peerj.5457

Hock R et al (2019) High mountain areas [Online]. Available: https://www.ipcc.ch/site/assets/uploads/sites/3/2019/11/06_SROCC_Ch02_FINAL.pdf. Accessed 27 Aug 2020

Hong S-Y, Noh Y, Dudhia J (2006) A new vertical diffusion package with an explicit treatment of entrainment processes. Mon Weather Rev 134:2318–2341. https://doi.org/10.1175/mwr3199.1

Hong SY, Lim JOJ (2006) The WRF single–moment 6–class microphysics scheme (WSM6). J Korean Meteor Soc 42: 129–151. https://www2.mmm.ucar.edu/wrf/users/phys_refs/MICRO_PHYS/WSM6.pdf

Hoyos N, Escobar J, Restrepo JC, Arango AM, Ortiz JC (2013) Impact of the 2010–2011 La Niña phenomenon in Colombia, South America: the human toll of an extreme weather event. Appl Geogr 39:16–25. https://doi.org/10.1016/j.apgeog.2012.11.018

Iacono MJ, Delamere JS, Mlawer EJ, Shephard MW, Clough SA, Collins WD (2008) Radiative forcing by long-lived greenhouse gases: calculations with the AER radiative transfer models. J Geophys Res. https://doi.org/10.1029/2008jd009944

IDEAM (2015) Atlas Climatológico de Colombia – Interactivo [Online]. Bogotá, D.C., Colombia. Accessed 3 Aug 2019

IDEAM (2017) Resultados Monitoreo de la deforestacion [Online]. Available: http://www.ideam.gov.co/documents/24277/0/Presentaci%97n+Estrategia+Integral+de+Control+a+la+Deforestaci%97n/173f79bf-3e68-4cbc-9387-80123d09b5e2. Accessed 29 June 2019

IDEAM (2018) Resulatdos monitoreo de la deforestacion [Online]. Available: http://documentacion.ideam.gov.co/openbiblio/bvirtual/023835/Resultados_Monitoreo_Deforestacion_2017.pdf. Accessed 29 June 2019

IDEAM (2019) Resultados Monitoreo de la deforestacion [Online]. Available: https://pidamazonia.com/sites/default/files/listado/Actualizacion_cifras2018FINALDEFORESTACION.pdf. Accessed 3 Oct 2019

IDEAM, PNUD, MADS, DNP, CANCILLERÍA (2017) Tercera Comunicación Nacional De Colombia a La Convención Marco De Las Naciones Unidas Sobre Cambio Climático (CMNUCC). Tercera Comunicación Nacional de Cambio Climático. Bogotá, Colombia

IPCC (2018) Summary for Policymakers. In: Masson-Delmotte V et al (eds) Global Warming of 1.5 °C. An IPCC special report on the impacts of global warming of 1.5 °C above pre-industrial levels and related global greenhouse gas emission pathways, in the context of strengthening the global response to the threat of climate change, sustainable development, and efforts to eradicate poverty

Jia G et al (2019) Land–climate interactions. Climate change and land: an IPCC special report on climate change, desertification, land degradation, sustainable land management, food security, and greenhouse gas fluxes in terrestrial ecosystems. Intergovernmental Panel on Climate Change

Jiménez PA, Dudhia J, González-Rouco JF, Navarro J, Montávez JP, García-Bustamante E (2012) A revised scheme for the WRF surface layer formulation. Mon Weather Rev 140:898–918. https://doi.org/10.1175/mwr-d-11-00056.1

Jiménez-Esteve B, Udina M, Soler MR, Pepin N, Miró JR (2018) Land use and topography influence in a complex terrain area: a high resolution mesoscale modelling study over the eastern Pyrenees using the WRF model. Atmos Res 202:49–62. https://doi.org/10.1016/j.atmosres.2017.11.012

Jin J, Miller NL, Schlegel N (2010) Sensitivity study of four land surface schemes in the WRF model. Adv Meteorol 2010:1–11. https://doi.org/10.1155/2010/167436

Kain JS (2004) The Kain-Fritsch convective parameterization: an update. J Appl Meteorol 43:170–181. https://doi.org/10.1175/1520-0450(2004)043%3c0170:Tkcpau%3e2.0.Co;2

Laux P, Nguyen PNB, Cullmann J, Kunstmann H (2017) Impacts of land-use/land-cover change and climate change on the regional climate in the central Vietnam. Land use and climate change interactions in central Vietnam. Springer

Lawrence D, Vandecar K (2015) Effects of tropical deforestation on climate and agriculture. Nat Clim Chang 5:27–36. https://doi.org/10.1038/nclimate2430

Lee S-J, Berbery EH (2012) Land cover change effects on the climate of the La Plata basin. J Hydrometeorol 13:84–102. https://doi.org/10.1175/jhm-d-11-021.1

Lejeune Q, Davin EL, Guillod BP, Seneviratne SI (2015) Influence of Amazonian deforestation on the future evolution of regional surface fluxes, circulation, surface temperature and precipitation. Clim Dyn 44:2769–2786. https://doi.org/10.1007/s00382-014-2203-8

Levavasseur G, Vrac M, Roche DM, Paillard D (2012) Statistical modelling of a new global potential vegetation distribution. Environ Res Lett. https://doi.org/10.1088/1748-9326/7/4/044019

Li X, Wang L, Guo X, Chen D (2017) Does summer precipitation trend over and around the Tibetan Plateau depend on elevation? Int J Climatol 37:1278–1284. https://doi.org/10.1002/joc.4978

Lin C-Y, Chua Y-J, Sheng Y-F, Hsu H-H, Cheng C-T, Lin Y-Y (2015) Altitudinal and latitudinal dependence of future warming in Taiwan simulated by WRF nested with ECHAM5/MPIOM. Int J Climatol 35:1800–1809. https://doi.org/10.1002/joc.4118

Llopart M, Reboita M, Coppola E, Giorgi F, da Rocha R, de Souza D (2018) Land use change over the amazon forest and its impact on the local climate. Water. https://doi.org/10.3390/w10020149

Lu S, Guo W, Xue Y, Huang F, Ge J (2021) Simulation of summer climate over Central Asia shows high sensitivity to different land surface schemes in WRF. Clim Dyn 57:2249–2268. https://doi.org/10.1007/s00382-021-05876-9

Mahmood R et al (2014) Land cover changes and their biogeophysical effects on climate. Int J Climatol 34:929–953. https://doi.org/10.1002/joc.3736

Meijide A, Shekhar Badu C, Moyano F, Tiralla N, Gunawan D, Knohl A (2018) Impact of forest conversion to oil palm and rubber plantations on microclimate and the role of the 2015 ENSO event. Agric For Meteorol 252:208–219. https://doi.org/10.1016/j.agrformet.2018.01.013

Nobre CA, Sellers PJ, Shukla J (1991) Amazonian deforestation and regional climate change. J Clim 4:957–988. https://doi.org/10.1175/1520-0442(1991)004%3c0957:ADARCC%3e2.0.CO;2

Nobre P, Malagutti M, Urbano DF, de Almeida RAF, Giarolla E (2009) Amazon deforestation and climate change in a coupled model simulation. J Clim 22:5686–5697. https://doi.org/10.1175/2009jcli2757.1

Núñez G (2014) Análisis del efecto de la modificación de la geodatabase (uso del suelo, elevación) en el clima simulado por Weather Research and Forecasting - WRF para la Sabana de Bogotá. [Master's Thesis, Universidad Nacional de Colombia]

Oliveira G, Brunsell NA, Moraes EC, Shimabukuro YE, Santos TV, Randow C, Aguiar RG, Aragao LEOC (2019) Effects of land-cover changes on the partitioning of surface energy and water fluxes in Amazonia using high-resolution satellite imagery. Ecohydrology. https://doi.org/10.1002/eco.2126

Pan Y et al (2011) A large and persistent carbon sink in the world's forests. Science 333:988–993. https://doi.org/10.1126/science.1201609

Paul S, Ghosh S, Oglesby R, Pathak A, Chandrasekharan A, Ramsankaran R (2016) Weakening of Indian summer monsoon rainfall due to changes in land use land cover. Sci Rep 6:32177. https://doi.org/10.1038/srep32177

Pepin N et al (2015) Elevation-dependent warming in mountain regions of the world. Nat Clim Chang 5:424–430. https://doi.org/10.1038/nclimate2563

Perugini L, Caporaso L, Marconi S, Cescatti A, Quesada B, de Noblet-Ducoudré N, House JI, Arneth A (2017) Biophysical effects on temperature and precipitation due to land cover change. Environ Res Lett. https://doi.org/10.1088/1748-9326/aa6b3f

Pleim JE, Xiu A (1995) Development and testing of a surface flux and planetary boundary layer model for application in mesoscale models. J Appl Meteorol 34:16–32. https://doi.org/10.1175/1520-0450-34.1.16

Posada-Marín JA, Rendón AM, Salazar JF, Mejía JF, Villegas JC (2018) WRF downscaling improves ERA-Interim representation of precipitation around a tropical Andean valley during El Niño: implications for GCM-scale simulation of precipitation over complex terrain. Clim Dyn 52:3609–3629. https://doi.org/10.1007/s00382-018-4403-0

Poveda G, Álvarez DM, Rueda ÓA (2011) Hydro-climatic variability over the Andes of Colombia associated with ENSO: a review of climatic processes and their impact on one of the Earth's most important biodiversity hotspots. Clim Dyn 36:2233–2249. https://doi.org/10.1007/s00382-010-0931-y

Powers JG et al (2017) The weather research and forecasting model: overview, system efforts, and future directions. Bull Am Meteor Soc 98:1717–1737. https://doi.org/10.1175/bams-d-15-00308.1

Prentice IC, Cramer W, Harrison SP, Leemans R, Monserud RA, Solomon AM (1992) Special paper: a global biome model based on plant physiology and dominance, soil properties and climate. J Biogeogr 19:117–134. https://doi.org/10.2307/2845499

Prevedello JA, Winck GR, Weber MM, Nichols E, Sinervo B (2019) Impacts of forestation and deforestation on local temperature across the globe. PLoS One 14:e0213368. https://doi.org/10.1371/journal.pone.0213368

PSL (2020) Multivariate ENSO index version 2 (MEI.v2) [Online]. NOAA. Physical Sciences Laboratory. Available: https://psl.noaa.gov/enso/mei/. Accessed 4 Oct 2019

Quesada B, Arneth A, de Noblet-Ducoudré N (2017a) Atmospheric, radiative, and hydrologic effects of future land use and land cover changes: a global and multimodel climate picture. J Geophys Res Atmos 122:5113–5131. https://doi.org/10.1002/2016jd025448

Quesada B, Devaraju N, Noblet-Ducoudré N, Arneth A (2017b) Reduction of monsoon rainfall in response to past and future land use and land cover changes. Geophys Res Lett 44:1041–1050. https://doi.org/10.1002/2016gl070663

Rangwala I, Miller JR (2012) Climate change in mountains: a review of elevation-dependent warming and its possible causes. Clim Change 114:527–547. https://doi.org/10.1007/s10584-012-0419-3

Ren HL, Zuo J, Deng Y (2018) Statistical predictability of Niño indices for two types of ENSO. Clim Dyn 52(9–10):5361–5382. https://doi.org/10.1007/s00382-018-4453-3

Robertson E (2019) The local biophysical response to land-use change in HadGEM2-ES. J Clim 32:7611–7627. https://doi.org/10.1175/jcli-d-18-0738.1

Saavedra M, Junquas C, Espinoza JC, Silva Y (2020) Impacts of topography and land use changes on the air surface temperature and precipitation over the central Peruvian Andes. Atmos Res. https://doi.org/10.1016/j.atmosres.2019.104711

Sampaio G, Nobre C, Costa MH, Satyamurty P, Soares-Filho BS, Cardoso M (2007) Regional climate change over eastern Amazonia

caused by pasture and soybean cropland expansion. Geophys Res Lett. https://doi.org/10.1029/2007gl030612

Sierra JP et al (2021) Deforestation impacts on Amazon-Andes hydroclimatic connectivity. Clim Dyn. https://doi.org/10.1007/s00382-021-06025-y

Skamarock WC et al (2008) A description of the advanced research WRF version 3. NCAR Tech Note NCAR/TN-475+STR. https://doi.org/10.5065/D68S4MVH

Skansi MDLM et al (2013) Warming and wetting signals emerging from analysis of changes in climate extreme indices over South America. Glob Planet Chang 100:295–307. https://doi.org/10.1016/j.gloplacha.2012.11.004

Snyder PK, Foley JA, Hitchman MH, Delire C (2004) Analyzing the effects of complete tropical forest removal on the regional climate using a detailed three-dimensional energy budget: an application to Africa. J Geophys Res Atmos. https://doi.org/10.1029/2003jd004462

Soares PMM, Cardoso RM, Miranda PMA, de Medeiros J, Belo-Pereira M, Espirito-Santo F (2012) WRF high resolution dynamical downscaling of ERA-interim for Portugal. Clim Dyn 39:2497–2522. https://doi.org/10.1007/s00382-012-1315-2

Song XP, Hansen MC, Stehman SV, Potapov PV, Tyukavina A, Vermote EF, Townshend JR (2018) Global land change from 1982 to 2016. Nature 560:639–643. https://doi.org/10.1038/s41586-018-0411-9

Spracklen DV, Garcia-Carreras L (2015) The impact of Amazonian deforestation on Amazon basin rainfall. Geophys Res Lett 42:9546–9552. https://doi.org/10.1002/2015gl066063

Sun X, Xue M, Brotzge J, McPherson RA, Hu X-M, Yang X-Q (2016) An evaluation of dynamical downscaling of Central Plains summer precipitation using a WRF-based regional climate model at a convection-permitting 4 km resolution. J Geophys Res Atmos 121:13801–13825. https://doi.org/10.1002/2016jd024796

Syktus J, Deo RC, McAlpine CA, McGowan HA, Phinn S (2007) Impact of land cover change on climate and El Niño in Australia. MODSIM 2007: International Congress on Modelling and Simulation. The University of Canterbury, Christchurch, New Zealand

Takahashi A, Kumagai TO, Kanamori H, Fujinami H, Hiyama T, Hara M (2017) Impact of tropical deforestation and forest degradation on precipitation over borneo island. J Hydrometeorol 18:2907–2922. https://doi.org/10.1175/jhm-d-17-0008.1

Teklay A, Dile YT, Asfaw DH, Bayabil HK, Sisay K (2019) Impacts of land surface model and land use data on WRF model simulations of rainfall and temperature over Lake Tana Basin, Ethiopia. Heliyon 5:e02469. https://doi.org/10.1016/j.heliyon.2019.e02469

Tewari M, Chen F, Wang W, Dudhia J, LeMone MA, Mitchell K, Ek M, Gayno G, Wegiel J, Cuenca RH (2004) Implementation and verification of the unified NOAH land surface model in the WRF model. 20th conference on weather analysis and forecasting/16th conference on numerical weather prediction.

Tölle MH, Engler S, Panitz H-J (2017) Impact of abrupt land cover changes by tropical deforestation on southeast Asian climate and agriculture. J Clim 30:2587–2600. https://doi.org/10.1175/jcli-d-16-0131.1

Urrutia R, Vuille M (2009) Climate change projections for the tropical Andes using a regional climate model: temperature and precipitation simulations for the end of the 21st century. J Geophys Res. https://doi.org/10.1029/2008jd011021

Vuille M, Bradley RS (2000) Mean annual temperature trends and their vertical structure in the tropical Andes. Geophys Res Lett 27:3885–3888. https://doi.org/10.1029/2000gl011871

Wang W et al (2017) WRF-ARW V3: User's Guide.

Wang Q, Fan X, Wang M (2016) Evidence of high-elevation amplification versus Arctic amplification. Sci Rep 6:19219. https://doi.org/10.1038/srep19219

Wang X, Tolksdorf V, Otto M, Scherer D (2020) WRF-based dynamical downscaling of ERA5 reanalysis data for high mountain Asia: towards a new version of the high Asia refined analysis. Int J Climatol 41:743–762. https://doi.org/10.1002/joc.6686

Winckler J, Reick CH, Pongratz J (2017) Robust identification of local biogeophysical effects of land-cover change in a global climate model. J Clim 30:1159–1176. https://doi.org/10.1175/jcli-d-16-0067.1

Zemp DC, Schleussner CF, Barbosa HMJ, Rammig A (2017) Deforestation effects on Amazon forest resilience. Geophys Res Lett 44:6182–6190. https://doi.org/10.1002/2017gl072955

Zhang H, Li Y, Gao X (2009) Potential impacts of land-use on climate variability and extremes. Adv Atmos Sci 26:840–854. https://doi.org/10.1007/s00376-009-8047-1